Journal of Turbomachinery, Volume 136, October 2014, Article number 101001
Accepted manuscript posted 21 May 2014, DOI: 10.1115/1.4027747

Industrial Gas Turbine Performance: Compressor Fouling and Online Washing

Uyioghosa Igie, Pericles Pilidis, Dimitrios Fouflias, Kenneth Ramsden and Panagiotis Laskaridis

Energy and Power Division

Cranfield University,

Bedfordshire, MK43 0AL, UK

email: u.igie@cranfield.ac.uk

tel: +44 (0) 1234 758382

ABSTRACT

Industrial gas turbines are susceptible to compressor fouling, which is the deposition and accretion of airborne particles or contaminants on the compressor blades. This paper demonstrates the blade aerodynamic effects of fouling through experimental compressor cascade tests and the accompanied engine performance degradation using TURBOMATCH, an in-house gas turbine performance software. Similarly, online compressor washing is implemented taking into account typical operating conditions comparable to industry high pressure washing.

The fouling study shows the changes in the individual stage maps of the compressor in this condition, the impact of degradation during part-load, influence of control variables and the identification of key parameters to ascertain fouling levels.

Applying demineralised water for 10 minutes, with a liquid-to-air ratio of 0.2%, the aerodynamic performance of blade is shown to improve, however most of the cleaning effect occurred in the first 5 minutes. The most effectively washed part of the blade was the pressure side, in which most of the particles deposited during the accelerated fouling. The simulation of fouled and washed engine conditions indicates 30% recovery of the lost power due to washing.

Keywords: compressor fouling, online washing, cascade blade aerodynamics and gas turbine performance simulation

INTRODUCTION

Modern advanced gas turbine compressor blades are becoming thinner and 3D twisted to achieve higher pressure ratios [1]. This improvement is accompanied by higher susceptibility to fouling due to the physical characteristics of the blades and a higher sensitivity as a result of the increased stage loading. Boyce and Latcovich [1] suggest that for these new advanced systems, the availability is down by 10% while the degradation rate is between 5% - 7% of the shaft power in the first 10,000 EOH. Though this is partly attributed to a number of other issues, it raises the need for ancillary equipment for retention or enhancement of engine performance during operation. There are a number of options available to achieve this. The strategy may include the use of filtration systems, compressor washing, evaporative cooling or inlet fogging (one or more of these).

The focus of this study is online compressor washing, which involves the injection of atomized droplets into the compressor at full or part-load. The philosophy behind online washing is that it is a proactive approach in mitigating fouling effects through regular wash, thereby maintaining the performance of the engine closer to optimum.

There are relatively few studies indicating the performance impact of online washing. Some of the notable studies include Syverud and Bakken [2], Boyce and Gonzalez [3], Stalder [4], Schneider et al. [5] and Kurz and Brun [6]. Published test findings often indicate the increase in power output after washing, without relating this to the lost output. This is however a cumbersome process mainly due to variability in load and ambient conditions that makes such analysis lengthy. The main point here is the estimation of “recovery of lost power” after washing, which can assist engine operators make informed performance based judgment in relation to the economics of their plant operation. To achieve this, with the understanding that the benefits of online washing can be site specific, careful assumptions could be made to provide outcomes that are more attainable in most operations. To accomplish this, only the first stage of the compressor model is considered to be washed in the performance simulation. This study also demonstrates the blade aerodynamic characteristic (e.g. blade trailing edge wakes and flow profile, flow coefficient and angles) changes that occur during fouling and after washing that is not possible to capture in a gas turbine compressor during operation.

EXPERIMENT

The compressor cascade test facility shown in Fig. 1 is a low-speed tunnel located in the Test House of Cranfield University. Compressor cascade experimental data provides insight on the complex flow condition in axial turbomachines. This 2D analysis consists of airfoils placed in rows to replicate a compressor stator blade effect [7]. Horlock [8] states that for compressors with large hub-to-tip ratio, cascade analysis is a close representation of the flow in the machine as the resulting radial velocity are small. The compressor cascade under investigation is a suction-type wind tunnel, with an inlet cross-sectional area of 0.0043 m^2 and mass flow of 5 kg/s. This corresponds to an inlet Mach number of 0.3 and Reynolds number of 3.8 x $10^{5.}$ There are 9 NACA 65(7)08 blades with a chord length of 60 mm and span length of 180 mm, all placed at a zero design incidence angle for higher static pressure rise. Fig. 2 shows these metallic blades (with an average surface roughness of 0.5 µm – based on k_{CLA}), which have an aspect ratio of 3. With this aspect ratio and number of blades employed, this specification conforms to the requirement for obtaining good two-dimensionality of the flow; that includes the removal of boundary layer effects on tunnel wall and end wall as recommended in Dixon [9] and earlier demonstrated in Pollard and Gostelow [10] to avoid flow interference and secondary vorticity. In addition to this, measurements taken in this study was at mid-span for the three middle blades that further eliminates such an influence. For these blades only their pitch-wise measurements were taken upstream and downstream. The measurements at these stations are along the traverse line, one-chord distance from the leading and trailing edge. Taking measurements at the specified chord distance is a generally acceptable convention in analysing two-dimensional cascade flows, especially downstream. This is because sufficient mixing of the flow downstream has occurred [11]. Fig. 3 indicates a reference point marked 0 mm along the traverse. This reference point is considered at the trailing passage between blade 4 and 5. Such approach is taken into account for expediency, nulling the three-hole probe in a relatively steady flow region rather than the trailing wake region of blade 5 (the cascade middle blade). Markings -40 mm and 120 mm indicate the range of traverse distance covered for the three middle blades with respect to the reference point. Upstream measurements were taken similarly, using a pitot-static tube.

When the three-hole probe was nulled on the yaw axis, it was observed that the nulling point angular uncertainty is ±1 ° (i.e. the uncertainty associated with measuring the flow). In total, 9 separate tests were carried out in which the clean, fouled and washed blade conditions were repeated 3 times respectively and non-dimensionalised. All measured pressures from both probes were filtered using 3 point moving averages. This output relative to the original values is in error below 0.1% in all cases and every line plot in the subsequent sub-section is averaged values of the 3 tests.

Fouling: Blade Aerodynamic Performance

The method of fouling presented in this subsection is that of an accelerated process that could have accrued over 2,000 EOH in a compressor depending on the environment. To investigate the effect of fouling on the blades, about 2 kg of organic flour was ingested via the intake of the wind tunnel at a low inlet Mach number of 0.04 (about 11 m/s). This involved dispersing the particles from a tray the width of the tunnel intake, slowly stroking a metal piece left to right of the intake. By doing so, it caused particle depositions on the blades that are fairly similar to the CFD model shown in Igie [12]. Attempts were made to ingest particles at the design inlet Mach 0.3, but only very few particles stuck on the blades despite the adhering fluid agent. The adhering fluid in use contains Acrylate Copolymer, which gives a strong hold to solid in contact. The middle three blades were initially sprayed and given about 2 minutes to dry slightly before fouling. The use of this sticky agent can be compared to a case of oil leakage or oily vapour in actual engines, which increases the particle deposition rate [13]. The range of particle sizes provided by the manufacturer that is ingested in the tunnel is provided in Table 14 of the Appendix. This indicates larger particles sizes that would be normally be captured by high efficiency filters, however these sizes (higher inertia) were used to accelerate fouling levels, as larger particles increases the cascade collection/capture efficiency [14,12] also demonstrated in Balan and Tabakoff [15]. In addition to this, it was important to obtain a fouled blade condition that is measurable, to be compared with the washed condition.

Blade 4, 5 and 6 particle deposition is indicated in Fig. 4 for the suction and pressure side respectively. This figure indicates the leftover of particles on the blade after the initial fouling shown in Fig. 28 of the Appendix, where it can be been seen that the pressure side is more fouled than the suction side. Most of the particle deposition on the pressure side is found to concentrate around mid-

chord up to the trailing edge with a maximum additional thickness of 1 mm. However the level of particle deposition demonstrated here had to be reduced due to the possibility of detachments of particles that could block the probes. This was achieved by running the cascade at the maximum speed which led to the final outcome presented in Fig. 4. The three fouled blades have fairly similar particle deposition on both suction and pressure sides, indicating the possibility to achieve good distribution of particles on the blades during particle ingestion.

The traverse non-dimensional velocity plot is indicated in Fig. 5, illustrating greater trailing passage velocity relative to the wake region for clean and fouled cases downstream. The profile in the wake region is normally expected to diminish or mix-out farther downstream due to mixing from the neighbouring higher trailing passage velocity. The figure also clearly shows that for the fouled blades, the passage velocity is greater as a result of the reduced effective blade-to-blade pitch (passage) caused by the physical presence of the particles on the blade. The roughness of the blades incites more turbulence in the flow, causing larger low wake velocity to be dissipated due to friction.

The reduced effective blade-to-blade pitch is not only a result of the physical presence of the particles, but also the increased boundary layer thickness that is accompanied. The diffusing effect of the stator blade is then compromised by a reduced area that often leads to static pressure decrease. Fig. 6 indicates lower normalised downstream static pressure for the fouled blades compared to the clean blades.

The total pressure loss coefficient is a useful parameter to quantify the mixing loss by the free stream trailing passage to the neighbouring low wake velocity region. As the magnitude of the low wake velocity increases by mixing, thus gradually becoming similar in magnitude to the passage flow (forming a more uniform flow), the average total pressure is reduced. Fig. 7 indicates greater loss coefficient in the wake region relative to the free stream as explained. That of the fouled blade is higher due to greater flow separation occurring as a result of increased boundary layer thickness caused by the increased surface roughness. The loss coefficient is defined in relation to both upstream and downstream pressures. Upstream total pressure reduces by the time the flow is downstream due to the blade profile loss. It can be observed from the clean blade plot that profile losses are inevitable; however the effects

are relatively minimal at design operation. Horlock [8] states that the difficulty of achieving flows free from separation over the blade surfaces has been the main reason the development of axial compressor lags behind turbine blade development. It is useful to present the losses in a descriptive context by using the mean values of the total pressure loss coefficient (ω) across the traverse for the middle three blades. Table 1 clearly indicates the values. The change in the total pressure loss coefficient would however depend on the blade profile type.

Apart from the downstream velocity, the change in exit flow angle of the blade can be used to describe the turbulence in the flow due to fouling. Fig. 8 indicates the exit flow angle for the clean and fouled blades, taken across the traverse. From previous discussions, the fact that downstream non-dimensional velocity and total pressure losses are higher for the fouled blade already infers greater exit flow angles. This is because a flow with more turbulent mixing has higher exit flow angle. The average difference in the exit flow angles between the clean and the fouled blade flow is 4.8 º and similar findings have been observed in Mal'tsev and Shakov [16].

Online Washing: Aerodynamic Performance

On-line compressor cascade blade washing was conducted after the connection of the wash kit which includes the pump, the wash liquid reservoir (tank), a pipe filter system and the nozzle (with its connecting support) shown in Fig. 9. The tank consists of a heat coil as shown in the top right of the figure, which ensures that the wash liquid can be heated. The containing liquid can also be pressurised to high pressures by adjusting the pump regulator. For the washing carried out, a number of procedures has been employed and are provided in Table 2.

For the experiment, the nozzle was placed at the inlet of the tunnel, along the vertical mid-span of the airfoil blades as shown in Fig. 9 (bottom-right). Washing was carried out for 10 minutes in total, using 7 litres of the demineralised water. The first 5 minutes of washing led to removal of particles from the blades which did not change much after another 5 minutes of washing (see Fig. 10). This infers that most of the cleaning occurred in the first 5 minutes. The pressure side of the washed blade is seen to be better washed than the suction side, as a lot more particles were removed on this part of the blade.

The reduced effectiveness of washing in the suction side after the peak suction (around 4% of the chord) can be attributed to the increased boundary layer thickness that shifts the airfoil transition point (or point of separation) towards the leading edge - meaning an earlier separation.

Although this cascade study does not completely capture some of the flow effects that occurs in actual fouling and washing processes (such as the centrifugal effects of the rotor, the nature of the foulant used and its interfacial forces and some of the complexities related to nozzle positioning and droplets trajectories), important flow phenomena have been obtained as shown subsequently, alongside indicative outcomes. There is a close similarity to Syverud et al. [17] for which an actual compressor was used and shows a higher susceptibility of fouling on the pressure side when compared to the suction side as obtained in this study. With the same engine, Syverud and Bakken [2] also shows that further increase in washing duration from 1 to 4 minutes has a negligible impact on washing effectiveness, which is consistent with the findings of this study despite the difference in the nature of foulant here for 5 to 10 minutes of washing as shown in Fig. 29 of the Appendix.

The plot of averaged total pressure loss coefficient is indicated in Fig. 11. The figure clearly shows a decrease in the losses for the washed blade compared to the fouled in the trailing wake region and passage as well. The mean value of the total pressure loss coefficient along the traverse is also calculated and compared to previous blade cases. These are presented in Table 3. Similarly, the exit flow angles were measured and presented alongside the clean and fouled blades shown in Fig. 12. This figure indicates a small reduction of the flow angle from the fouled blade after washing. This improvement is found to be 1.3 º on average.

STAGE PERFORMANCE FROM CASCADE ANALYSIS

The equivalent stage performance from measurement of the blade characteristics in the previous sections can be estimated applying Howell's method. This involves applying correction factors to the two-dimensional cascade data of the mean diameter blade, to achieve actual mean stage performance [18]. The correction factors applied are due to three-dimensional effects like annulus wall boundary layer, tip and axial clearances and wakes from preceding blade rows obtained by extensive test on a full scale multi-stage compressor and single stage fan. These losses are depicted in Fig. 13.

The validated work of Howell [18] proposes that the overall drag coefficient of a stage is the sum of the profile, secondary and annulus drag as follows:

$$C_D = C_{Dp} + C_{Da} + C_{Ds} \tag{1}$$

The profile drag loss arises from blade skin friction and it is directly obtained from cascade experiments. The profile drag coefficient is

$$C_{Dp} = \frac{s}{c}\left(\frac{\Delta P_s}{1/2\rho V_1^2}\right)\frac{\cos^3\alpha_m}{\cos^2\alpha_1} \tag{2}$$

Stage annulus loss accounts for wall friction. The referred study demonstrates that for a compressor with 90% stage efficiency, approximately 2% of its loss is due to annulus effect. The annulus wall drag coefficient is calculated as

$$C_{Da} = 0.02\frac{s}{h} \tag{3}$$

while the trailing vortices, viscous dissipation of induced resultant velocities as well as other three-dimensional separation in the flow constitutes secondary loss and calculated by

$$C_{Ds} = 0.018C_L^2 \tag{4}$$

C_L is the lift coefficient derived as

$$C_L = 2\frac{s}{c}\cos\alpha_m(\tan\alpha_1 - \tan\alpha_2) \quad (5)$$

where

$$\tan\alpha_m = 0.5(\tan\alpha_1 + \tan\alpha_2) \quad (6)$$

With these parameters, the stage or polytropic efficiency that relates to the blade aerodynamic performance is calculated as

$$\eta_p = 1 - \left\{\frac{2}{\sin(2\alpha_m)} \times \frac{C_D}{C_L}\right\} \quad (7)$$

The flow coefficient, a measure of the mass flow is

$$\left(\frac{U}{V_a}\right)^{-1} = \phi = \frac{1}{(\tan\alpha_1 + \tan\alpha_2)} \quad (8)$$

The stage loading coefficient is

$$\psi = \frac{\Delta H}{U^2} = \lambda\phi(\tan\alpha_1 - \tan\alpha_2) \quad (9)$$

The outcomes of this procedure are presented in Table 4. As shown, the drag coefficient increases with fouling, that is mainly due to increased wall friction caused by higher blade roughness. This is accompanied by lower lift and higher mean angles (mainly influence by higher exit flow angle).The polytropic efficiency obtained for the clean blade is 92%, which is typical for an axial compressor stage. Similarly the flow coefficient indicated is within an expected range. A work done factor (λ) of 0.99 is applied for the single stage compressor [19] to calculate the stage loading coefficient. It is observed that with fouling the stage loading reduces however there is an improvement in all the stated parameters after washing.

The percentage reductions in the stage polytropic efficiency and flow coefficient (fouled and washed blades in relation to clean) is subsequently applied on the first stage of the gas turbine compressor (engine model in the next section) to simulate degraded engine conditions.

In many fouled compressors, the front stages are known to have the most particle deposition. This mechanism is discussed in details in Kurz and Brun [20]. To obtain a more indicative fouled compressor with fouling effects in more than one stage, the relationship between the roughness levels of the first three stages of a fouled compressor presented in Melino et al. [21] has been applied. This has been used to estimate the drop in stage polytropic efficiency and flow coefficient for stage two and three, based on the relative roughness to stage one. Fouflias et al. [22] demonstrates almost linear relationship between increasing blade roughness and drop polytopic efficiency and flow coefficient to support this assumption. The outcome of this is summarised in the Table 5.

For the washed compressor, the reduction in polytropic efficiency and flow coefficient that relates to the experiment is applied on the first stage. Only this stage of the three fouled stages is assumed to be washed and hence the other stages retain their degradation as shown in Table 6.

GAS TURBINE PERFORMANCE

The performance of a single-shaft engine has been modelled and simulated using TURBOMATCH, a Cranfield University in-house software. The clean, fouled and washed steady-state engine conditions have been simulated and presented here. The simple cycle configuration considered is shown in Fig. 14. The model investigated here is a 7.9 MW engine with Turbine Entry Temperature (TET) as the control variable (with no VIGV).

The operating point for which the engine is designed is specified in Table 7. These include specified design point objectives at ISA condition derived from published engine specifications for an actual engine. Some of the unspecified outcomes (parameters) are the fuel flow and EGT.

The simulation code used consists of standard compressor maps embedded in the software that allows for map scaling. The individual stage operating point on their map is determined based on their calculated scaling factors shown in Eqs. (10) to (12). The numerator in these equations are the specified design point pressure ratio, stage isentropic efficiency and flow coefficient (non-dimensional mass flow capacity), while their denominator is the standard map corresponding values. The calculation of the operating conditions also involves mass and energy balance in the engine model to satisfy mass flow compatibility between the compressor and the turbine. This is achieved at convergence when matching the components. The surge margin of the individual stages of the compressor is specified at the design point.

$$prsf = \frac{pr_{Dp} - 1}{pr_{Dp\,Map} - 1} \tag{10}$$

$$etasf = \frac{\eta_{isDp}}{\eta_{isDpMap}} \tag{11}$$

$$wasf = \frac{\phi_{Dp}}{\phi_{DpMap}} \tag{12}$$

The steady-state surge margin for a compressor depends on the engine configuration and requirement of a given application [17]. Walsh and Fletcher [23] indicate that the surge margin for the individual stages of a compressor applicable to power generation is between 15-20%. For most compressors designs, the first stage with the highest pressure rise usually has the smallest surge margin relative to the middle and back stages [24]. For this model the same scheme has been followed by specifying the surge margin with the values shown in Table 8.

It is important to state that there are currently no general rules available in the public domain, indicating the surge margin variation for the stages of an axial compressor, as this is a proprietary information. Nonetheless, the surge margin is mathematically expressed in Eq. (13).

$$SM = \frac{pr_{surge} - pr_{working}}{pr_{working}} \tag{13}$$

Off-Design Performance: Fouled and Washed Engine

To obtain the degraded engine condition, the input variables of percentage change in stage isentropic efficiency ($\Delta\eta_{is}\%$) and flow coefficient ($\Delta\phi\%$) are applied to the design engine model. This operation is achieved through the following relations:

$$\eta_{is(\deg)} = (1 - \Delta\eta_{is}\%) \times etasf \times \eta_{isMap} \tag{14}$$

$$\phi_{(\deg)} = (1 - \Delta\phi\%) \times wasf \times \phi_{Map} \tag{15}$$

Fouled Engine Condition:

The fouled engine condition was simulated applying degradation levels indicated on Table 5. Changes in the characteristic maps for the first stage are highlighted in Figs. 15 and 16. These figures

shows the design speed line (N = 1.0) which indicates the design point pressure ratio and stage efficiencies respectively. When fouling occurs, the speed line is seen to change. For the constant shaft speed engine model, this is an indication of a changed map due to stage rematching. There is a shift in the operating point towards the left as a result of mass flow reduction and a corresponding downward drop in the operating point due to stage efficiency reduction. Subsequent fouled stages also show this change, to a lesser magnitude due to relatively less degradation levels. That of the second stage is indicated in Figs 17 and 18.

The unfouled stages suffer only the mass flow deficit from the front stages, forcing them to also operate at lower CMF. Similar to the fouled stages, the operating point shifts towards the left, but as these subsequent stages have their stage or aerodynamic efficiency the same, their maps remains unchanged. The left shift of the operating point on the same map translates to an increase in pressure ratio or loading of these subsequent stages. This is illustrated in Figs. 19 and 20 for the 4^{th} stage.

Figure 21 summarises the percentage changes in pressure ratio for all the stages, indicating pressure ratio reduction in the fouled front stages and small increase in the unfouled stages. There is an overall reduction in the compressor pressure ratio, as the drop in the initial stage pressure ratios exceeds the small increase in the back stages. The compressor component surge margin at steady-state infact improves due to the overall pressure ratio reduction.

The impact of fouling on the overall engine performance relative to the clean engine as a percentage is presented in Table 9. As observed, there is a reduction in all the performance parameters except the compressor discharge temperature which is explained in latter part of this paper. The mass flow and pressure ratio reduction are of the similar magnitude as observed in other studies [25]. The most significant reduction is the power output, while the overall compressor efficiency is the least. There is also a fuel flow reduction of 2.78% to maintain the TET.

Applying the same level of degradation at part-load (5.0 MW and TET – 1100 K) the following reductions in performance indicated in Table 10 is obtained. The table indicates that comparing the

clean engine part-load operation to its degraded condition, the impact of fouling is relatively more severe than if the same level of deterioration occurred at full-load. This is mainly due to the lower thermal efficiency at part-load operations, for which an additional reduction in fuel flow due to fouling (at constant TET) leads to more significant loss.

When operating at part-load and further away from the EGT limit, it is more convenient to run the engine based on load control (constant power). For this operation, the fuel flow would increase to maintain the power output in a fouled condition. This also increases the EGT and TET. Table 11 indicates that at part-load when the clean engine power output is 5.0 MW, the fuel flow increases by 3.05% while the TET rises by 2.55% (which is about 28 K rise in temperature). At full load, such increase can reduce/consume the creep life of the turbine blade quickly since the operation is closer to the EGT limit.

Stage-by-stage sensitivity to fouling and key indicators

To observe the influence of individual stage fouling on the overall engine performance, a stage-by-stage fouling sensitivity study is conducted up to the 5th stage. Table 12 shows the degraded performance of the engine with fouling at the first, third and fifth stage, simulated independently. From Fig. 22 it can be observed that the effect of fouling on the power output and overall engine performance is more severe on the first stage than subsequent stages. This is mainly due to the fact that the first stage has the highest pressure ratio and residual effect affects more stages. The effect on the third stage is greater than the fifth stage for the same reason; however the penalty on compressor efficiency reduction is greater than the mass flow reduction in such condition. A similar outcome was obtained in a previous study by Millsaps et al. [26] for a baseline three-stage compressor model with assumed uniform roughness on both rotor and stator. Fig. 22 also indicates that of all the parameters, the power output drops the most. To detect fouling for front stage fouling, it can be observed that the CDT isn't a reliable parameter. This is because there may be little or no change in CDT depending on the percentage change in compressor efficiency and fouling location. From Eq. (16), it is important to note that CDT is also affected by pressure ratio.

A reduced pressure ratio reduces the CDT due to lesser air compression. This is an opposing effect to the accompanied compressor efficiency reduction that increases CDT. Hence CDT increases when compressor efficiency reduction is more significant than mass flow (or pressure ratio). This is proven in Fig. 22, which shows increase in CDT from the third stage. This increase is by 1 K as shown on Table 12. Aker and Saravanmuttoo [27] indicate a similar outcome when fouling occurs after the first 20% of the compressor stages.

$$CDT = CIT\left[1+\frac{1}{\eta_c}\left(OPR^{\left(\frac{\gamma-1}{\gamma}\right)}-1\right)\right] \quad (16)$$

The most sensitive parameters to determine fouling would be based on the first stage since in most cases the front stage has to be fouled for fouling to exist in subsequent stages. The figure above also infers that change in power output, OPR and mass flow are better indicators of fouling effects. The intake depression has also been described as a sensitive parameter to detect fouling and independent of the engine control mode [17], however the approach is applicable to fixed geometry machines.

Washed Engine Condition

The change in the first stage characteristic map after washing is shown in Fig. 23 that represents the washed stage one. As shown, there is a shift of the speed line from the fouled stage speed line towards that of the clean stage on the right hand side. This is an indication of an improvement in the corrected mass flow. There is a rise in the pressure ratio shown at the higher operating point on the washed stage speed line. Much smaller improvement is observed in the second stage pressure ratio as shown in Fig. 24. This is simply because only the first stage is considered to be washed. Nevertheless a small residual effect of the improvement is observed in stage two pressure ratios. The back stages retained approximately similar pressure ratio increase as in the fouled compressor, though their exit total pressure improved. This improvement in the stage exit pressure is highlighted in Figs. 25 and 26 where the first two front stages, a middle stage and the last stage have been selected. The higher exit total pressure obtained in the last stage (ten) of the washed compressor therefore translates

to higher CDP and OPR (same inlet conditions). Improvements in the first stage efficiency was also obtained as shown in Fig. 27, however subsequent stage efficiency remained the same as in the fouled case.

The overall performance of the washed engine is indicated in Table 13 which shows improvements in all the performance parameters. At the design point TET, the power reduction in the washed engine relative to the clean engine is 3.06%. This is in contrast to the fouled engine which shows 4.37% power drop. It therefore infers that approximately 30% of the lost power is recovered after washing based on Eq. (17).

$$R_{P.lost} = \left[1 - \frac{P_{w.clean} - P_{w.washed}}{P_{w.clean} - P_{w.\,fouled}}\right] \times 100 \qquad (17)$$

CONCLUSIONS

In summary, this study has given an account of the aerodynamic and thermodynamic impacts of compressor blade fouling and on-line washing.

The use of Howell's method in calculating the stage efficiency indicates the applicability of the hypothesis, obtaining a typical stage efficiency of 92% for the clean blades. The fouled and washed blades analysis shows 3.8% and 1.7% reductions in the stage efficiency respectively (with respect to the clean blade). From the experimental results, a reasonable value of 0.531 is estimated as the flow coefficient for the clean blade and this method is applied in obtaining the changes due to fouling and after washing.

The impact of fouling in the first three stages of the compressor model shows that the maps of these stages changes; shifting towards the left hand side downwards to a lower corrected mass flow, pressure ratio and stage efficiency. The map of the unfouled stages remained unchanged; however the effect of reduced mass flow from earlier fouled stages shifts their operating point to a lower corrected mass flow. This causes their pressure ratios to increase with a reduction in their surge margins. As the decrease in pressure ratios in the fouled stages outweighs the increases in the unfouled stages, there is an overall pressure ratio reduction. These lead to a reduction in the power output by 4.37% and thermal efficiency by 1.56%.

Washing the blades in intervals showed that most of the cleaning occurred in the first 5 minutes of washing, from visual inspection. The most effectively washed part of the blade is the pressure side, where most of the particles deposited. This occurred especially around mid-span position where the nozzle was placed. The root of the blades remained almost the same before and after washing due to the lack of sufficient spray coverage in this region. Measurements taken after washing showed an improvement in all the aerodynamic performance parameters as a result of the widening of the effective pitch.

Washed engine condition has been investigated, assuming only the first stage is cleaned (using experimental results). The simulation shows that the first stage characteristics map shifts towards the clean stage map. This signifies an improvement in the stage corrected mass flow, pressure ratio and stage efficiency. The increased pressure ratio and exit delivery pressure of the first stage causes subsequent stage exit total pressure to increase. The accumulative effect is an increase in the overall pressure ratio that causes the power output, thermal efficiency to increase. The outcome of this study indicates a 30% recovery of the lost power due to on-line washing. This estimate is considered to be a representative value, since there is the uncertainty that there could be possible evaporation of demineralised water, possible redeposition of foulants in the rear stages and that a small proportion of

the injected droplet may be centrifuged towards the compressor casing. Hence the assumption that only the first stage among the three fouled stages is washed is thought to be prudent. This value can enable engine operators estimate the profitability and viability of applying online washing for their engine.

This investigation also infers two key outcomes of on-line washing, which are; enhancing power output and retarding the loss in performance due to fouling. The greatest benefits accrue when the washing is initiated immediately following overhaul/engine commissioning; when implemented proactively, with the appropriate nozzle position, droplet size distribution and liquid injection pressure.

ACKNOWLEDGMENT

The authors owe gratitude to Paul Lambart, Russell Gordon, Andy Lewis, and Jonathon O' Donnell of R-MC Power Recovery Ltd for the technical support and funding.

NOMENCLATURE

c Blade chord length, mm

C_D Drag coefficient

C_{Da} Annulus drag coefficient

C_{Dp} Profile drag coefficient

C_{Ds} Drag coefficient for secondary losses

C_L Lift coefficient

etasf Isentropic efficiency scaling factor

h Blade height (span), mm

ΔH Enthalpy change, J/kg

k_{CLA} Centre-line average roughness, µm

K Kelvin, K

M Mass flow of air, kg/s

pr Stage pressure ratio

prsf Pressure ratio scaling factor

P Total pressure, Pa

P_s Static pressure, Pa

P_w Power output, MW

$R_{P.lost}$ Recovery of lost power, %

s Blade-to-blade pitch, mm

U Blade mean speed, m/s

V Velocity, m/s

V_a Axial velocity, m/s

wasf Non-dimensional mass flow scaling factor

Greek Symbols

α Flow angle, deg

Δ Change

η Efficiency, %

ρ Density of air, kg/m^3

µm Micrometer

ϕ Flow coefficient

ψ Stage loading coefficient

λ Blockage or work done factor

ω Total pressure loss coefficient

γ Specific heat ratio

Subscripts

1 Cascade blade inlet

2 Cascade blade outlet

amb Ambient

c Compressor

clean Clean

deg Degraded, degree

Dp Design point

fouled Fouled

is Isentropic

m Mean

Map Map

p Polytropic,

surge Surge

th Thermal efficiency

tot Total

washed Washed

working Working

Acronyms

2D Two dimensional

3D Three dimensional

CDP Compressor discharge pressure, Pa

CDT Compressor discharge temperature, K

CIT Compressor inlet temperature, K

CFD Computational fluid dynamics

CMF Corrected mass flow, kg/s

EOH Engine operating hours

EGT Exhaust gas temperature, K

ISA International standard atmosphere

MW Mega Watt

NACA National Advisory Committee for Aeronautics

OPR Overall pressure ratio

PS Pressure side

SM Surge margin

SS Suction side

TET Turbine entry temperature, K

VIGV Variable inlet guide vane

APPENDIX

REFERENCES

[1] Boyce, M., and Latcovich, J., 2002, "Condition Monitoring and its Effects on the Life of New Advanced Gas Turbines," ASME-IGTI Glob. Gas Turbine News, **42**(3), pp. 32.

[2] Syverud, E., and Bakken, L., 2007, "Online Water Wash Tests of GE J85-13," J. Turbomach., **129**(1), pp. 136-142. DOI: 10.1115/1.2372768.

[3] Boyce, M., and Gonzalez, F., 2005, "A Study of On-Line and Off-Line Turbine Washing to Optimize the Operation of a Gas Turbine Washing to Optimize the Operation of a Gas Turbine," J. Eng. Gas Turbines Power, **129**(1), pp. 114-122. DOI: 10.1115/1.2181180.

[4] Stalder, J., 2001, "Gas Turbine Compressor Washing State of the Art: Field Experiences," J. Eng. Gas Turbines Power, **123**(2). pp. 362-370. DOI: 10.1115/1.1361108.

[5] Schneider, E., Demircioglu, S., Franco, S., and Therkorn, D., 2010, "Analysis of Compressor On-Line Washing to Optimize Gas Turbine Power Plant Performance," J. Eng. Gas Turbines Power, **132**(6), 062001. DOI:10.1115/1.4000133.

[6] Kurz, R., and Brun, K., 2000, "Degradation in Gas Turbine Systems," J. Eng. Gas Turbines Power, **123**(1), pp. 70-77. DOI:10.1115/1.1340629.

[7] Boyce, M., 2006, Gas turbine engineering handbook. Boston: Gulf Professional Pub.

[8] Horlock, J., 1973, Axial Flow Compressors: Fluid Mechanics and Thermodynamics. R. E. Krieger Publishing Company.

[9] Dixon, S., 1998, Fluid Mechanics and Thermodynamics of Turbomachinery, Elsevier.

[10] Pollard, D., and Gostelow, J., 1967, "Some Experiments at Low Speed on Compressor Cascades," J. Eng. Gas Turbines Power, **89**(3), pp. 427-436. DOI:10.1115/1.3616709.

[11] Gostelow, J., 1984, Cascade aerodynamics. Pergamon Press.

[12] Igie, U., 2011, "Degraded Gas Turbine Performance and Economic Analysis: Compressor Fouling and On-Line Washing for Industrial Prime Movers," Ph.D. Thesis, Cranfield University, United Kingdom.

[13] Meher-Homji, C., and Bromley, A., 2004, "Gas Turbine Axial Compressor Fouling and Washing," Proceedings of the 33rd Turbomachinery Symposium.

[14] Song, T., Song, J., Kim, T., Kim, J., and Ro., S., 2005, "An Analytical Approach to Predicting Particle Deposit by Fouling in the Axial Compressor of the Industrial Gas Turbine," Proc. Inst. Mech. Eng. Part J. Power Energy, **219**(3), pp. 203-212. DOI: 10.1243/095765005X7547.

[15] Balan, C., and Tabakoff, W., 1983, "Effects of Particle Presence on the Incompressible Inviscid Flow through a Two Dimensional Compressor Cascade," ASME 28th International Gas Turbine Conference, Arizona, United States.

[16] Malt'sev, Y., and Shakov, V., 1989, "Influence of Roughness of Deposits in Compressor Cascade on Flow Lag Angle," *Sov. Aeronaut.*, 32(3), pp. 90–92.

[17] Syverud, E., Brekke, O., and Bakken, L., 2007, "Axial Compressor Deterioration Caused by Saltwater Ingestion," J. Turbomach., **129**(1), pp. 119–126. DOI:10.1115/1.2219763.

[18] Howell, A., 1945, "Fluid Dynamics of Axial Compressors," Proc. Inst. Mech. Eng., **153**(1), pp. 441-452. DOI:10.1243/PIME_PROC_1945_153_049_02.

[19] Howell, A., and Bonham, R., 1950, "Overall and Stage Characteristics of Axial-Flow Compressors," Proc. Inst. Mech. Eng., **163**(1), pp. 235-248. DOI: 10.1243/PIME_PROC_1950_163_026_02.

[20] Kurz, R., and Brun, K., 2012, "Fouling Mechanisms in Axial Compressors," J. Eng. Gas Turbines Power, **134**(3), 032401.DOI:10.1115/1.4004403.

[21] Melino, F., Morini, M., Peretto, A., Pinelli, M., and Ruggero Spina, P., 2012, "Compressor Fouling Modeling: Relationship Between Computational Roughness and Gas Turbine Operation Time," J. Eng. Gas Turbines Power, **134**(5), 052401. DOI:10.1115/1.4004739.

[22] Fouflias, D., Gannan, A., Ramsden, K., Pilidis, P., Mba, D., Texeira, J., Igie, U., and Lambart, P., 2010, "Experimental Investigation of the Influence of Fouling on Compressor Cascade Characteristics and Implications for Gas Turbine Engine Performance," Proc. Inst. Mech. Eng. Part A, J. Power Energy, **224**(7), pp. 1007-1018. DOI: 10.1243/09576509JPE992.

[23] Walsh, P., and Fletcher, P., 2004, "Gas Turbine Performance," Malden, MA: Blackwell Science.

[24] Falck, N., 2008, "Axial Flow Compressor Mean Line Design," M.Sc. Thesis, Lund University, Sweden.

[25] Tarabrin, A., Schurovsky, A., Bodrov, A., and Stalder, J., 1998, "An Analysis of Axial Compressor Fouling and a Blade Cleaning Method," J. Turbomach., **120**(2), pp. 256-261. DOI:10.1115/1.2841400.

[26] Millsaps, K., Baker, J., and Patterson, J., 2004, “Detection and Localization of Fouling in a Gas Turbine Compressor From Aerothermodynamic Measurements,” ASME Paper No. GT2004-54173.

[27] Aker, G., and Saravanamutto, H., 1989, "Predicting Gas Turbine Performance Degradation Due to Compressor Fouling Using Computer Simulation Techniques," J. Eng. Gas Turbines Power, **111**(2), pp. 343-350. DOI:10.1115/1.3240259.

LIST OF FIGURES

Fig. 1 The compressor cascade tunnel

Fig. 2 The cascade clean blades

Fig. 3 Upstream and downstream traverse locations

Fig. 4 Suction and pressure side of the blade (fouled)

Fig. 5 Downstream non-dimensional velocity

Fig. 6 Normalised downstream static pressure

Fig. 7 Total pressure loss coefficient

Fig. 8 Downstream exit flow angles

Fig. 9 Washing kit: pump (top-left), tank (top right), nozzle spray (bottom-left), nozzle on support (bottom-right)

Fig. 10 Blade suction and pressure side after washing

Fig. 11 Total pressure loss coefficient (all cases)

Fig. 12 Exit flow angle (all cases)

Fig. 13 Three-dimensional losses in an axial stage

Fig. 14 A simple gas turbine

Fig. 15 Stage (1) map of pr versus CMF

Fig. 16 Stage (1) map of efficiency versus CMF

Fig. 17 Stage (2) map of pr versus CMF

Fig. 18 Stage (3) map of pr versus CMF

Fig. 19 Stage (4) map of pr ratio versus CMF

Fig. 20 Stage (4) map of efficiency versus CMF

Fig. 21 % Changes in pressure ratio for various stages

Fig. 22 Change in performance due to fouling for various fouling stage locations

Fig. 23 Stage (1) map of pr versus CMF (all case)

Fig. 24 % Changes in pr for all stages (degraded)

Fig. 25 Exit total pressure for stage 1 and 2 (all cases)

Fig. 26 Exit total pressure for stage 5 and 10 (all cases)

Fig. 27 Stage (1) map of efficiency versus CMF (all cases)

Fig. 28 Suction (left) and pressure (right) side of the blade after fouling

Fig. 29 Blade suction and pressure side after 5 and 10 minutes of washing respectively

LIST OF TABLES

Table 1 Mean total pressure loss coefficient

Table 2 Details of the on-line washing scheme

Table 3 Mean total pressure loss coefficient

Table 4 Stage aerodynamic performance (all cases)

Table 5 % reduction in poly. efficiency and flow coefficient (Fouled compressor)

Table 6 % reduction in poly. efficiency and flow coefficient (Washed compressor)

Table 7 Summary of the design point performance

Table 8 Surge margin for various compressor stages

Table 9 Effect of fouling on performance at design point

Table 10 Effect of fouling on performance at part-load

Table 11 Effect of fouling on performance at part-load (Constant power)

Table 12 Stage-by-stage sensitivity to fouling on overall engine performance (TET-1300K)

Table 13 Effect of washing on performance at design constant TET (1300K)

Table 14 Range of particle size composition

Table 1 Mean total pressure loss coefficient

Parameter	Clean blades	Fouled blades
$\bar{\omega}$	0.056	0.092

Table 2 Details of the on-line washing scheme

Variables	Value/Description
Wash liquid	demineralised water
Wash liquid heated temp.	50ºC
Wash liquid injection pressure	90bars

Liquid-to-air ratio by mass flow	0.002
Volume of wash liquid used	7 litres
Wash duration	5 mins × 2
Nozzle type	flat fan
Nozzle aperture area	0.08 mm^2
Droplet size	50 to 150 μm

Table 3 Mean total pressure loss coefficient

Parameter	Clean blades	Fouled blades	Washed blades
$\overline{\omega}$	0.056	0.092	0.072

Table 4 Stage aerodynamic performance (all cases)

Parameters	Clean	Fouled	Washed
Drag coefficient C_D	0.029	0.034	0.031
Lift coefficient C_L	0.68	0.58	0.62

Mean angle α_m	43.3	44.4	44.1
Polytropic efficiency η_P	92%	88%	90%
Flow coefficient ϕ	0.531	0.510	0.517
Stage loading coefficient ψ	0.308	0.257	0.274

Table 5 % reduction in poly. efficiency and flow coefficient (Fouled compressor)

Fouled stages		
Stage number	**η_p reduction (%)**	**ϕ reduction (%)**
1	3.77	3.93

2	1.73	1.80
3	0.85	0.89

Table 6 % reduction in poly. efficiency and flow coefficient (Washed compressor)

Washed and Fouled stages		
Stage number	**η_p reduction (%)**	**ϕ reduction (%)**
1	1.70	2.63

2	1.73	1.80
3	0.85	0.89

Table 7 Summary of the design point performance

Design Objectives	Value	Design Objectives	Value
Intake			
Ambient temperature	288.15 K	Ambient pressure	1.01 bar

Total pressure recovery	99%	Intake mass flow	30 kg/s
Compressor			
Compressor efficiency	88%	Compressor pressure ratio	11.54
Compressor exit temperature	618 K	Number of stages	10
Burner			
Combustion efficiency	99%	Burner pressure loss	5%
Fuel flow	0.56 kg/s	Thermal efficiency	33%
Turbine and Fixed Area Nozzle			
Turbine inlet temperature	1300 K	Turbine efficiency	89%
Net power output	7.9 MW	Exhaust gas temperature	780 K

Table 8 Surge margin for various compressor stages

Stage no.	**1**	**2**	**3**	**4**	**5**	**6**	**7**	**8**	**9**	**10**
Surge margin (%)	15.0	15.6	16.1	16.7	17.2	17.8	18.3	18.9	19.4	20.0

Table 9 Effect of fouling on performance at design point

Performance Parameter (TET-1300K)	% Reduction
Mass flow	2.82%
Overall compressor efficiency	1.56%

Overall pressure ratio	2.71%
Fuel flow	2.78%
Compressor delivery temperature	**unchanged**
Power output	4.37%
Thermal efficiency	1.64%

Table 10 Effect of fouling on performance at part-load

Performance Parameter (TET-1100K)	**% Reduction**
Mass flow	2.82%

Overall compressor efficiency	1.56%
Overall pressure ratio	2.46%
Fuel flow	2.89%
Compressor delivery temperature	**unchanged**
Power output	5.32%
Thermal efficiency	2.50%

Table 11 Effect of fouling on performance at part-load (Constant power)

Performance Parameter (TET-1100K)	**Change**

Mass flow **reduction**	2.82%
Overall compressor efficiency **reduction**	1.46%
Overall pressure ratio **reduction**	1.80%
Fuel flow **increase**	3.05%
Compressor delivery temperature	**negligible rise**
Power output	unchanged
Thermal efficiency **reduction**	0.57%

Table 12 Stage-by-stage sensitivity to fouling on overall engine performance (TET-1300K)

Cases	M (kg/s)	η_c (%)	OPR	CDT (K)	P_w	η_{th} (%)
Clean	30.00	88.36	11.54	618	7.90	32.54
Stage 1	29.34	87.20	11.30	618	7.64	32.15
Stage 3	29.83	87.66	11.46	619	7.76	32.23
Stage 5	29.95	87.86	11.51	619	7.81	32.30

Table 13 Effect of washing on performance at design constant TET (1300K)

Performance Parameter	% Increase
Mass flow	0.83%
Overall compressor efficiency	0.46%
Overall pressure ratio	0.80%
Compressor delivery temperature	**unchanged**
Power output	1.35%
Thermal efficiency	0.51%

APPENDIX

Table 14 Range of particle size composition

Particle size	% Composition
>150 µm	7.0
>132 µm	6.2
>112 µm	9.2
>40 µm	47.0
>25 µm	10.9
>15 µm	9.8
<15 µm	9.9

.

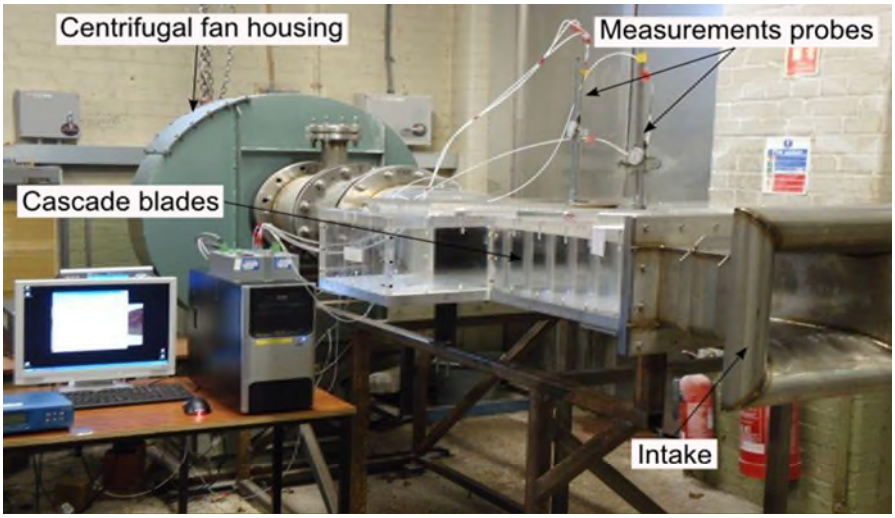
Centrifugal fan housing
Measurements probes
Cascade blades
Intake

Fig1.tiff

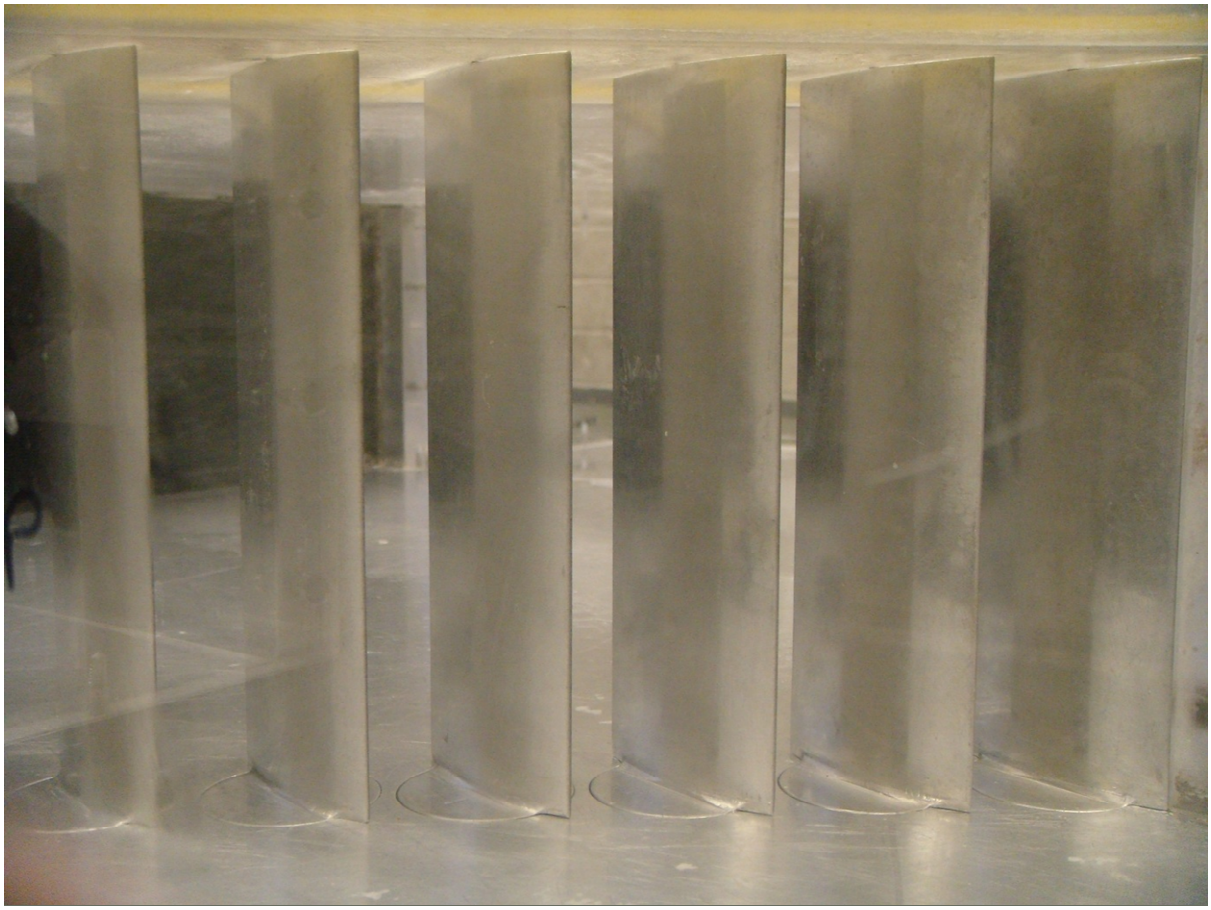

Fig2.tiff

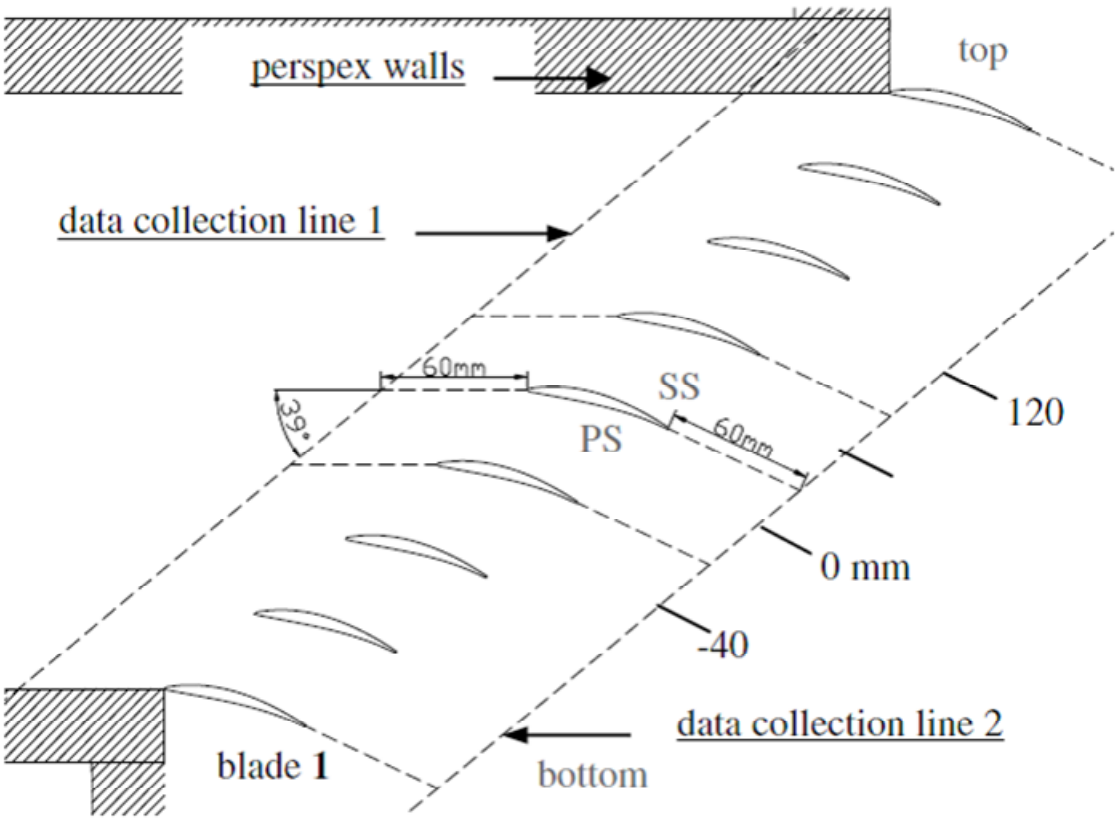
perspex walls
top
data collection line 1
60mm
SS
39°
PS
60mm
120
0 mm
-40
data collection line 2
blade 1
bottom

Fig3.tiff

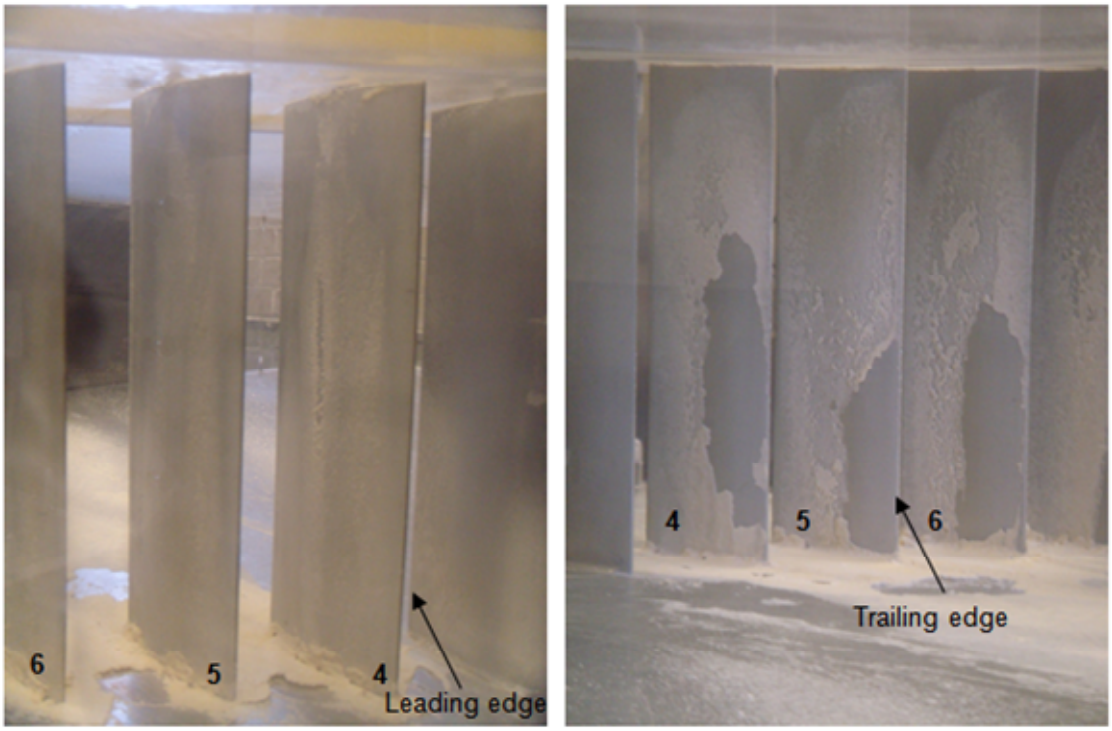

Fig4.tiff

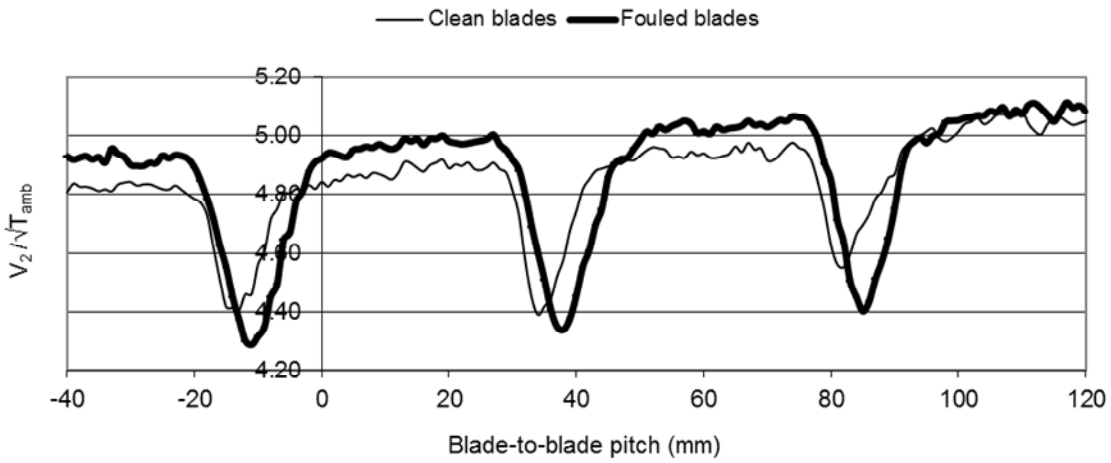
Clean blades
Fouled blades
5.20
5.00
4.80
4.60
4.40
4.20
$V_2/\sqrt{T_{amb}}$
-40
-20
0
20
40
60
80
100
120
Blade-to-blade pitch (mm)

Fig5.tiff

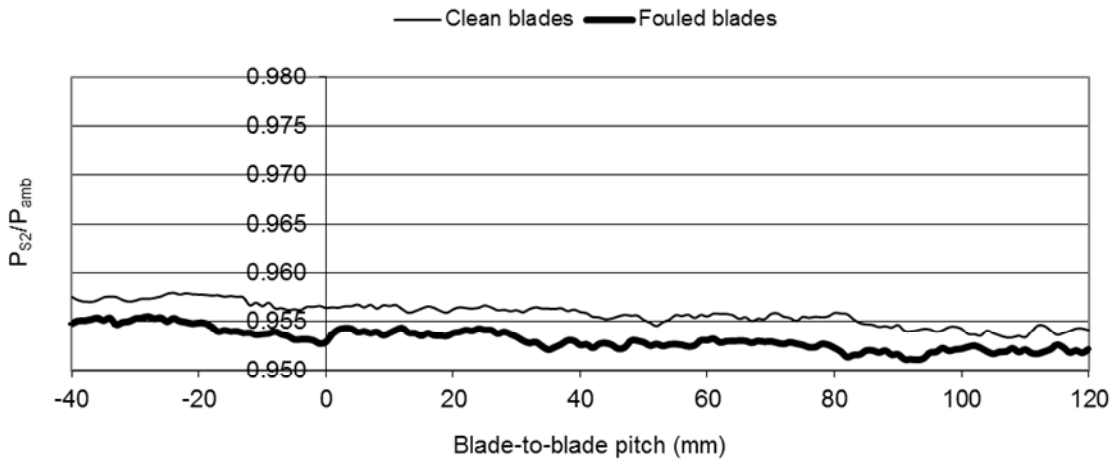
Clean blades
Fouled blades
0.980
0.975
0.970
0.965
0.960
0.955
0.950
P_{S2}/P_{amb}
-40
-20
0
20
40
60
80
100
120
Blade-to-blade pitch (mm)

Fig6.tiff

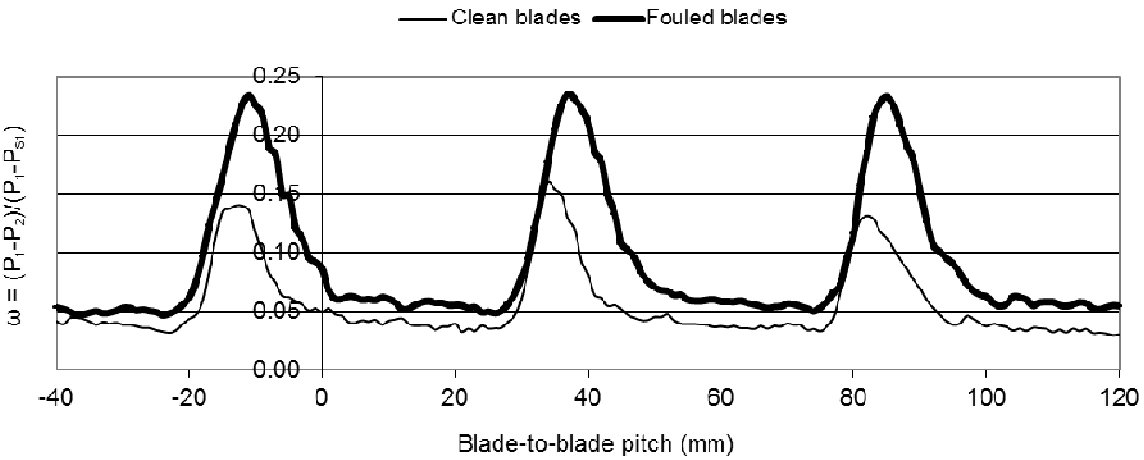
Clean blades
Fouled blades
0.25
0.20
0.15
0.10
0.05
0.00
ω = (P1-P2)/(P1-Ps1)
-40
-20
0
20
40
60
80
100
120
Blade-to-blade pitch (mm)

Fig7.tiff

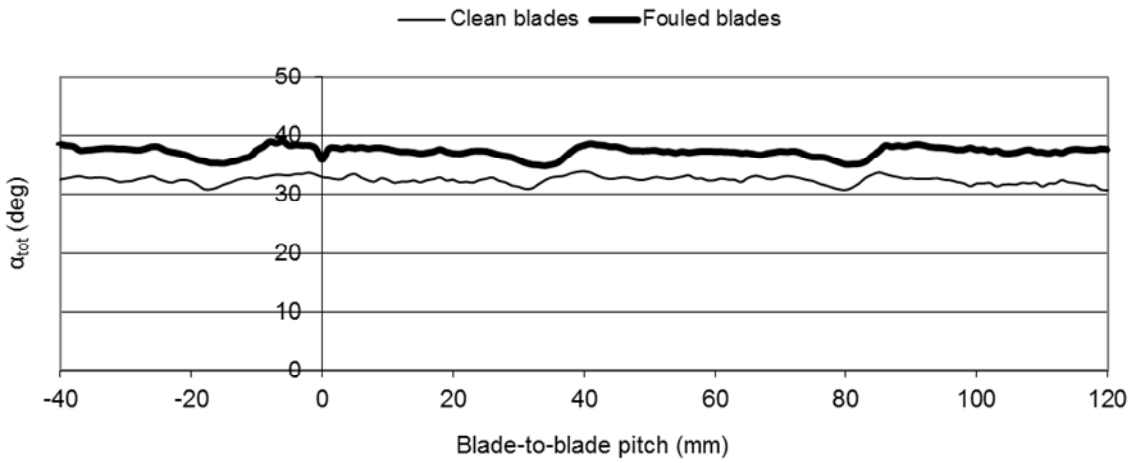
Clean blades
Fouled blades
50
40
30
20
10
0
α_{tot} (deg)
-40
-20
0
20
40
60
80
100
120
Blade-to-blade pitch (mm)

Fig8.tiff

Fig9.tiff

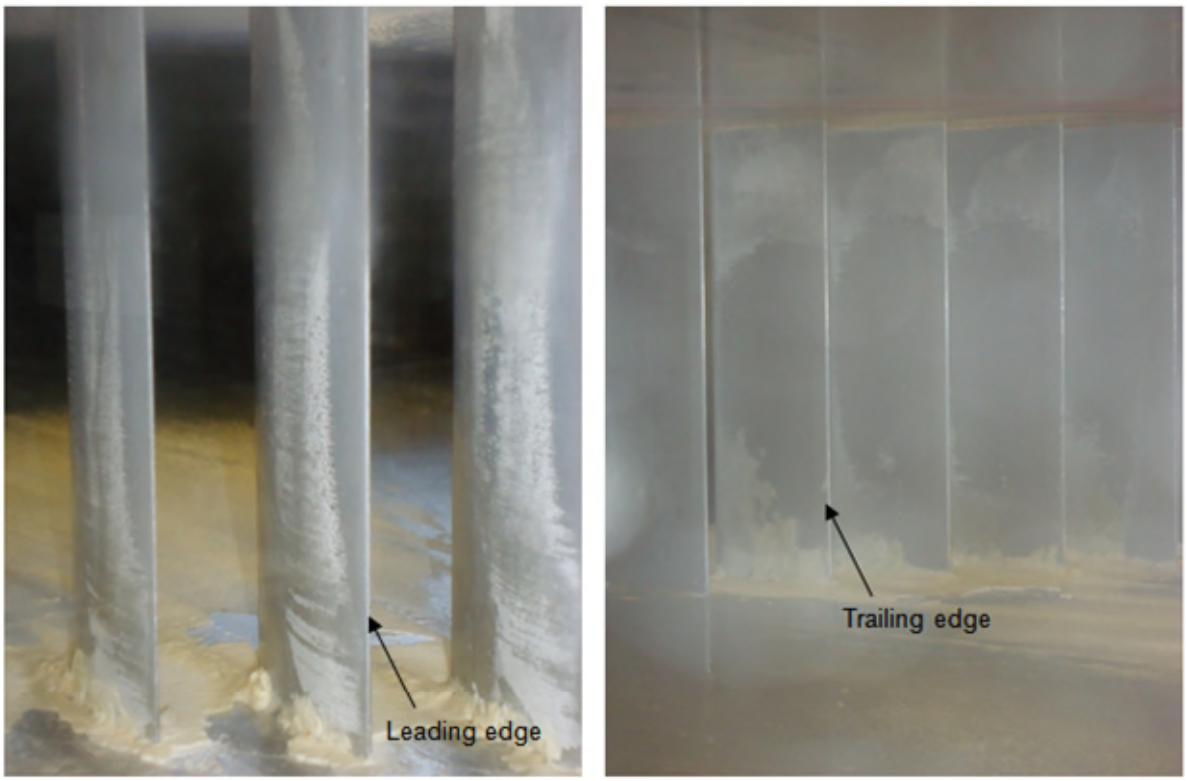

Fig10.tiff

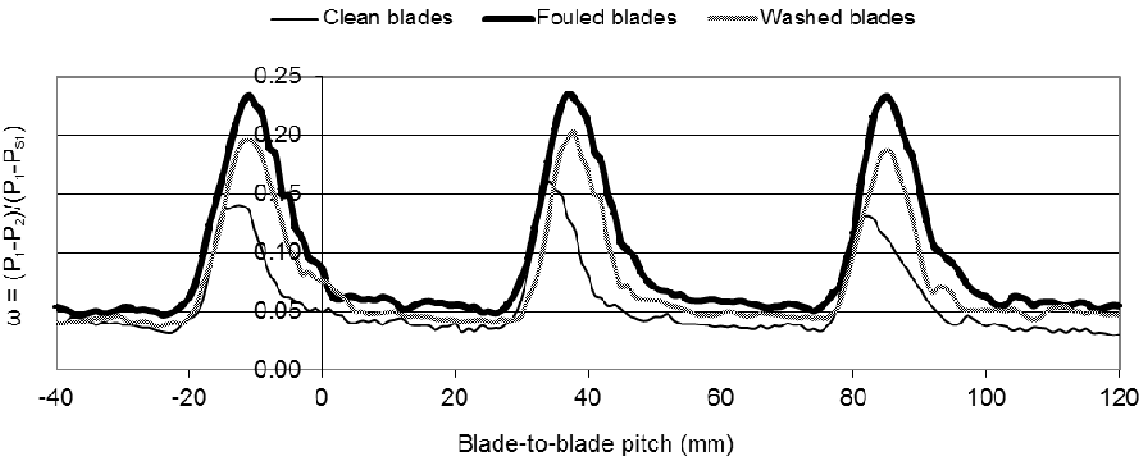
Clean blades
Fouled blades
Washed blades
0.25
0.20
0.15
0.10
0.05
0.00
-40
-20
0
20
40
60
80
100
120
Blade-to-blade pitch (mm)

Fig11.tiff

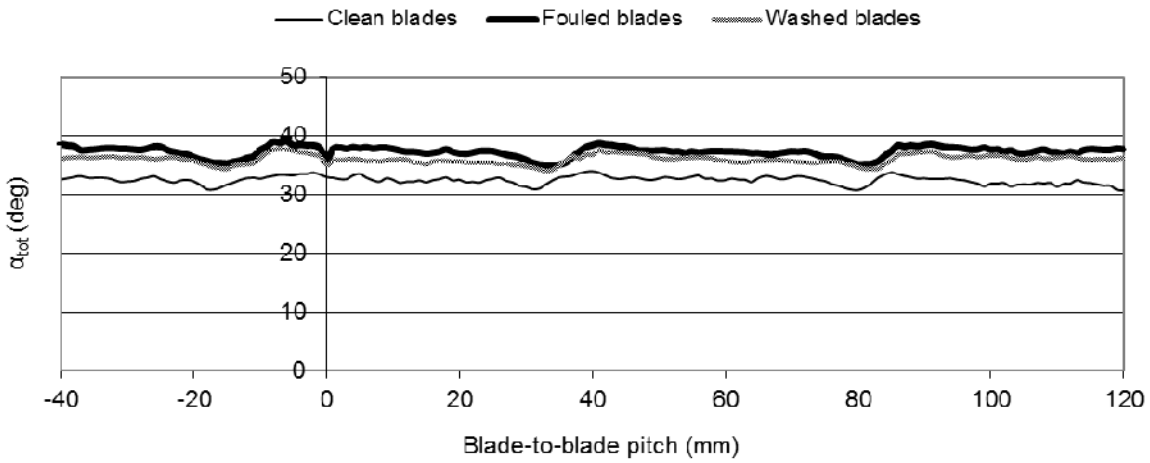
Clean blades
Fouled blades
Washed blades
50
40
30
20
10
0
α_{tot} (deg)
-40
-20
0
20
40
60
80
100
120
Blade-to-blade pitch (mm)

Fig12.tiff

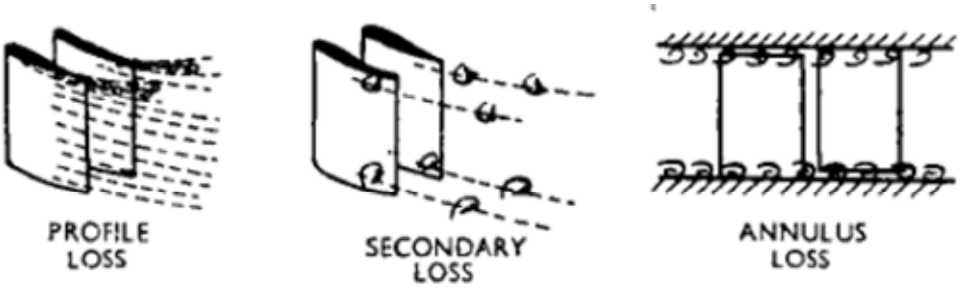

Fig13.tiff

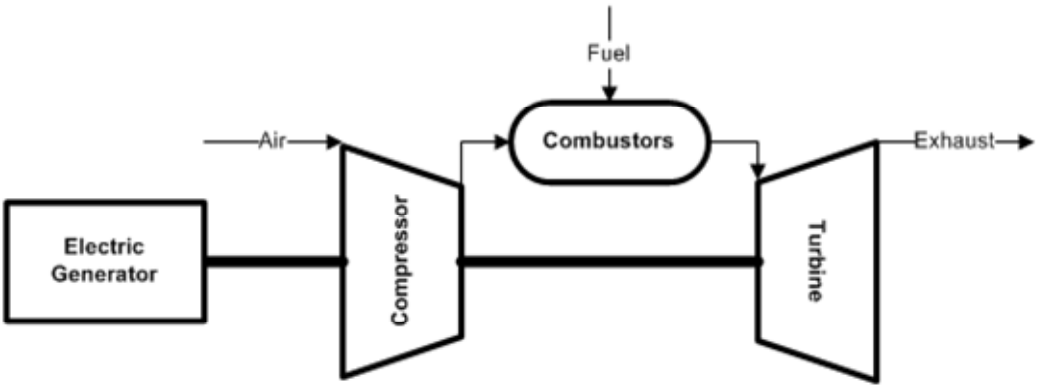
Fuel
Air
Combustors
Exhaust
Electric Generator
Compressor
Turbine

Fig14.tiff

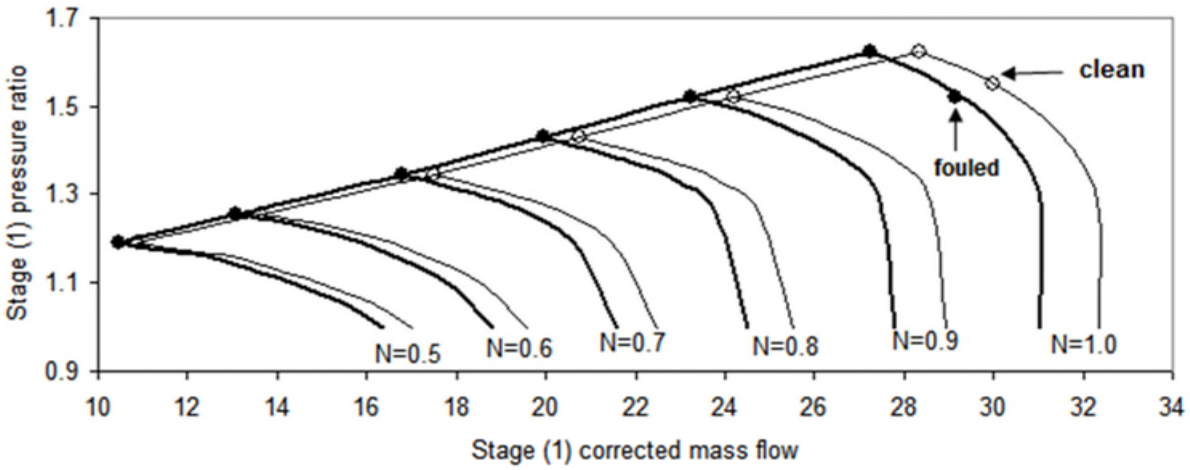
Stage (1) pressure ratio
1.7
1.5
1.3
1.1
0.9
10
12
14
16
18
20
22
24
26
28
30
32
34
Stage (1) corrected mass flow
clean
fouled
N=0.5
N=0.6
N=0.7
N=0.8
N=0.9
N=1.0

Fig15.tiff

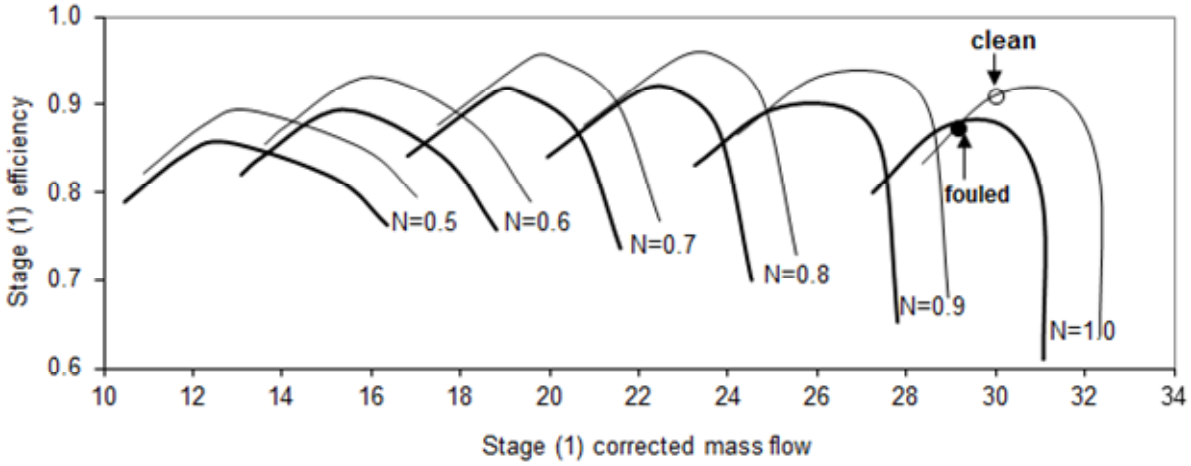
1.0
0.9
0.8
0.7
0.6
Stage (1) efficiency
10
12
14
16
18
20
22
24
26
28
30
32
34
Stage (1) corrected mass flow
clean
fouled
N=0.5
N=0.6
N=0.7
N=0.8
N=0.9
N=1.0

Fig16.tiff

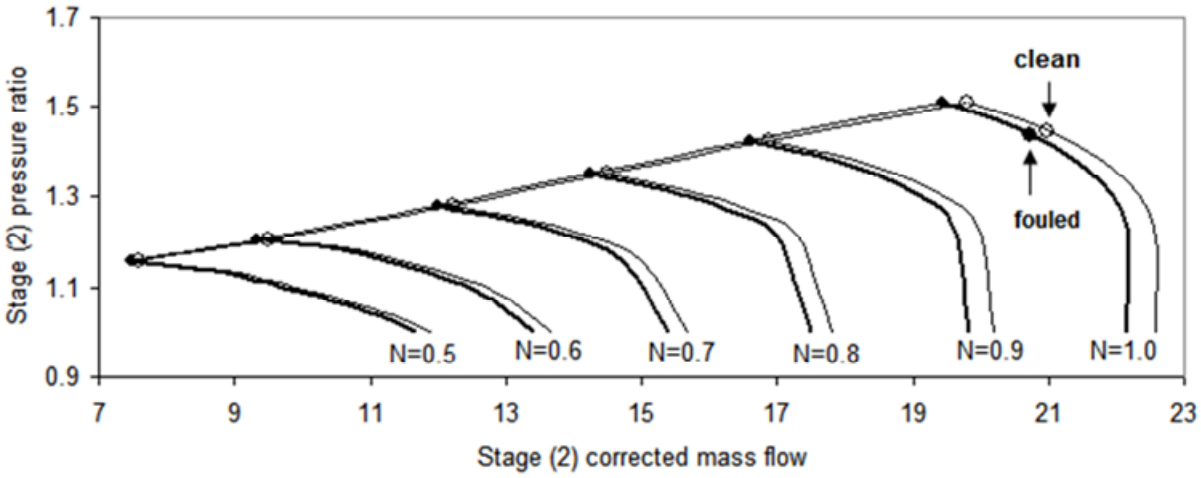
1.7
1.5
1.3
1.1
0.9
Stage (2) pressure ratio
7
9
11
13
15
17
19
21
23
Stage (2) corrected mass flow
clean
fouled
N=0.5
N=0.6
N=0.7
N=0.8
N=0.9
N=1.0

Fig17.tiff

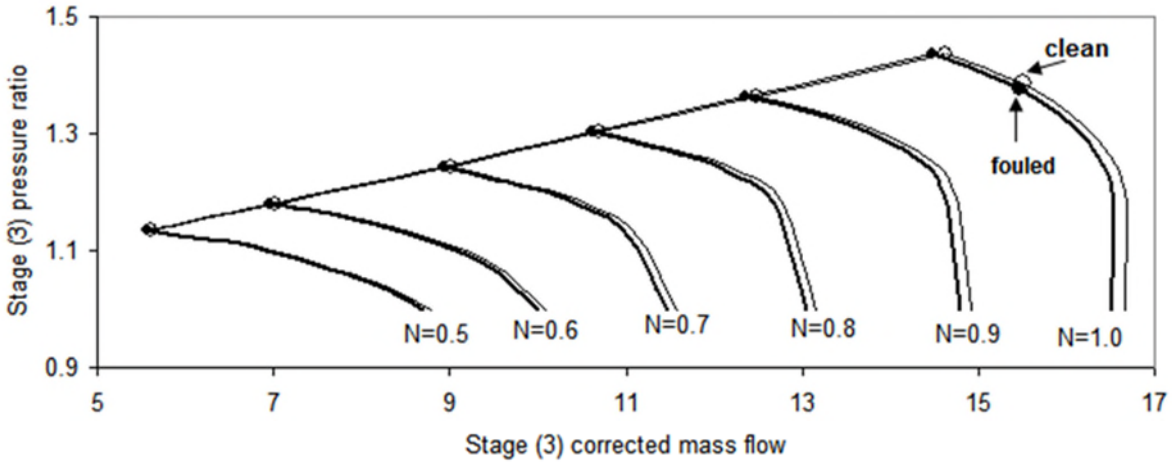
1.5
1.3
1.1
0.9
Stage (3) pressure ratio
5
7
9
11
13
15
17
Stage (3) corrected mass flow
clean
fouled
N=0.5
N=0.6
N=0.7
N=0.8
N=0.9
N=1.0

Fig18.tiff

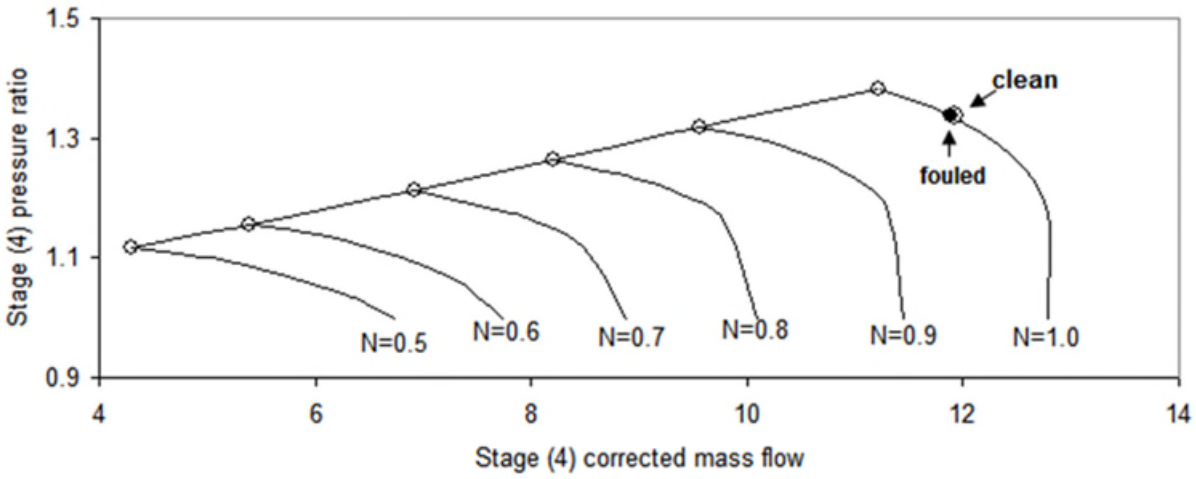
1.5
1.3
1.1
0.9
Stage (4) pressure ratio
4
6
8
10
12
14
Stage (4) corrected mass flow
clean
fouled
N=0.5
N=0.6
N=0.7
N=0.8
N=0.9
N=1.0

Fig19.tiff

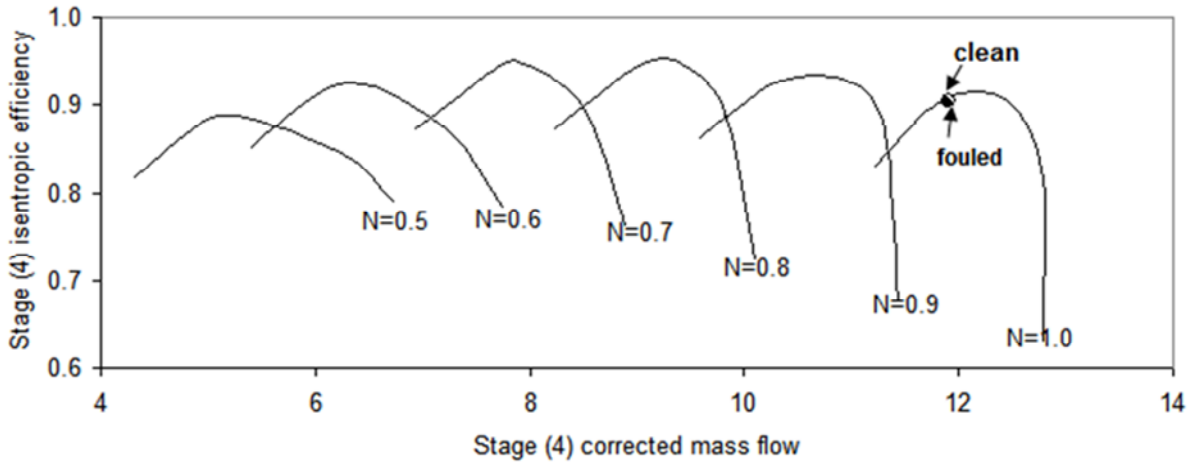
1.0
0.9
0.8
0.7
0.6
Stage (4) isentropic efficiency
4
6
8
10
12
14
Stage (4) corrected mass flow
clean
fouled
N=0.5
N=0.6
N=0.7
N=0.8
N=0.9
N=1.0

Fig20.tiff

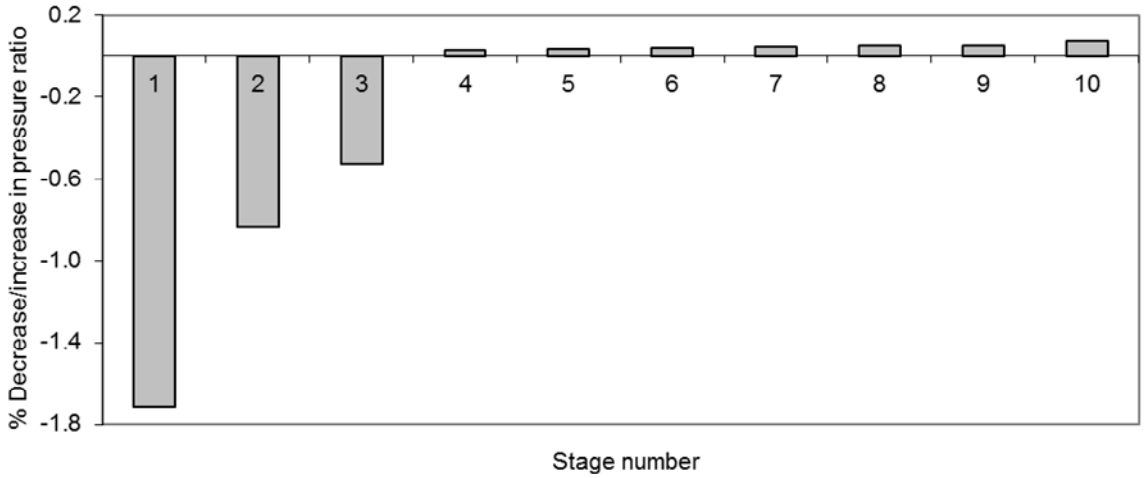
0.2
-0.2
-0.6
-1.0
-1.4
-1.8
% Decrease/increase in pressure ratio
1
2
3
4
5
6
7
8
9
10
Stage number

Fig21.tiff

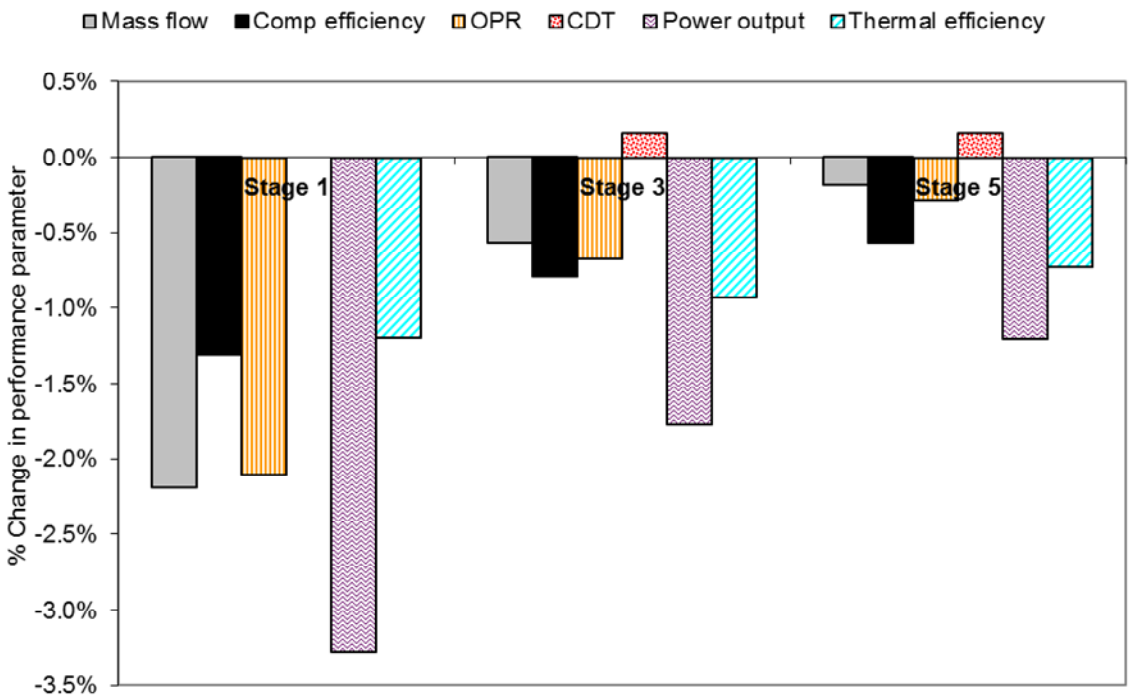
Mass flow
Comp efficiency
OPR
CDT
Power output
Thermal efficiency
0.5%
0.0%
-0.5%
-1.0%
-1.5%
-2.0%
-2.5%
-3.0%
-3.5%
% Change in performance parameter
Stage 1
Stage 3
Stage 5

Fig22.tiff

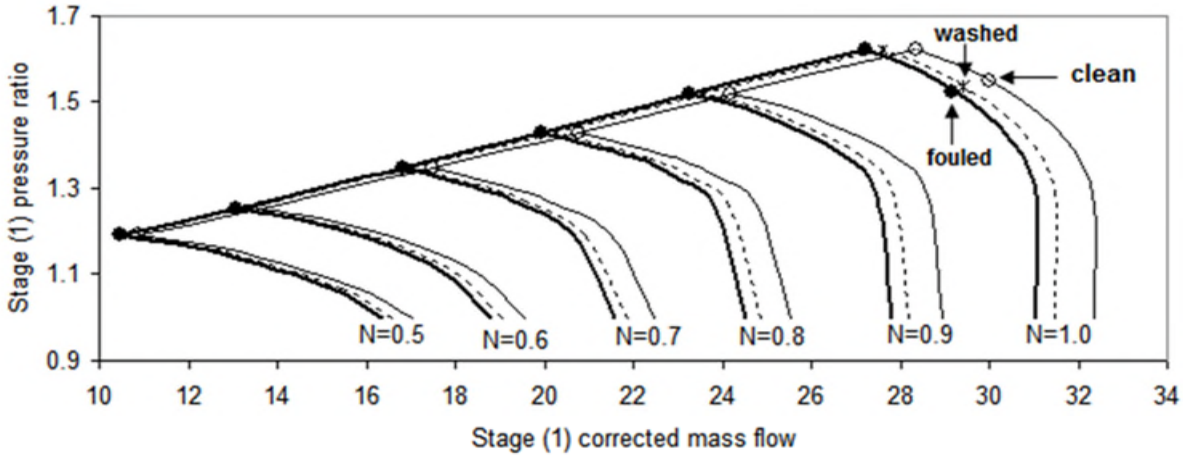
Stage (1) pressure ratio
1.7
1.5
1.3
1.1
0.9
10
12
14
16
18
20
22
24
26
28
30
32
34
Stage (1) corrected mass flow
washed
clean
fouled
N=0.5
N=0.6
N=0.7
N=0.8
N=0.9
N=1.0

Fig23.tiff

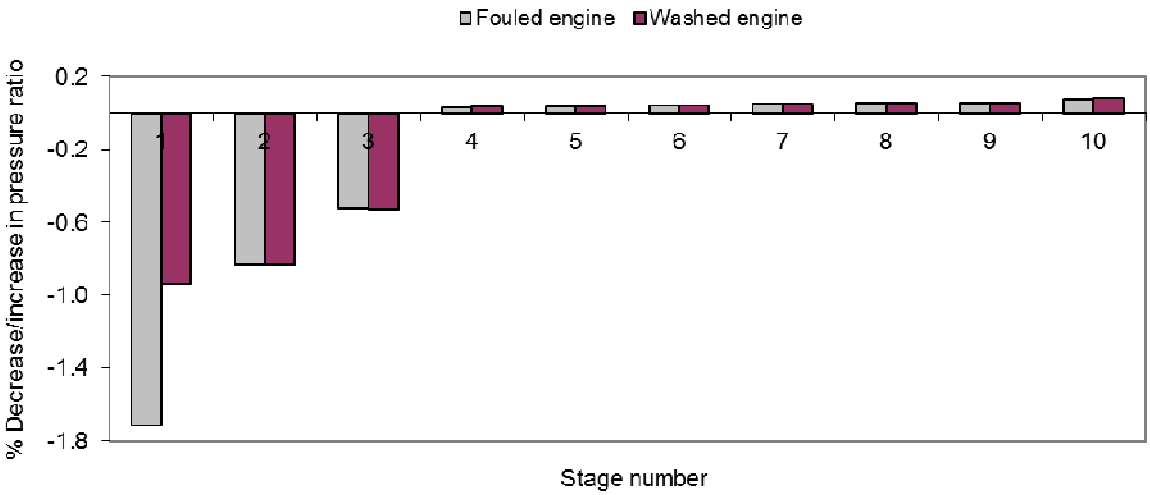
Fouled engine
Washed engine
% Decrease/increase in pressure ratio
0.2
-0.2
-0.6
-1.0
-1.4
-1.8
1
2
3
4
5
6
7
8
9
10
Stage number

Fig24.tiff

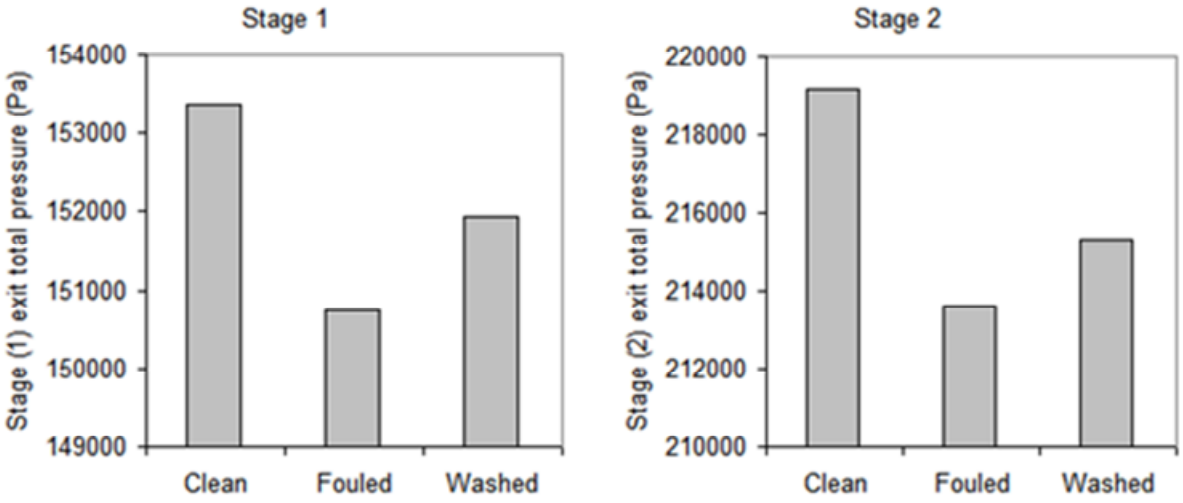
Stage 1
Stage (1) exit total pressure (Pa)
154000
153000
152000
151000
150000
149000
Clean
Fouled
Washed
Stage 2
Stage (2) exit total pressure (Pa)
220000
218000
216000
214000
212000
210000
Clean
Fouled
Washed

Fig25.tiff

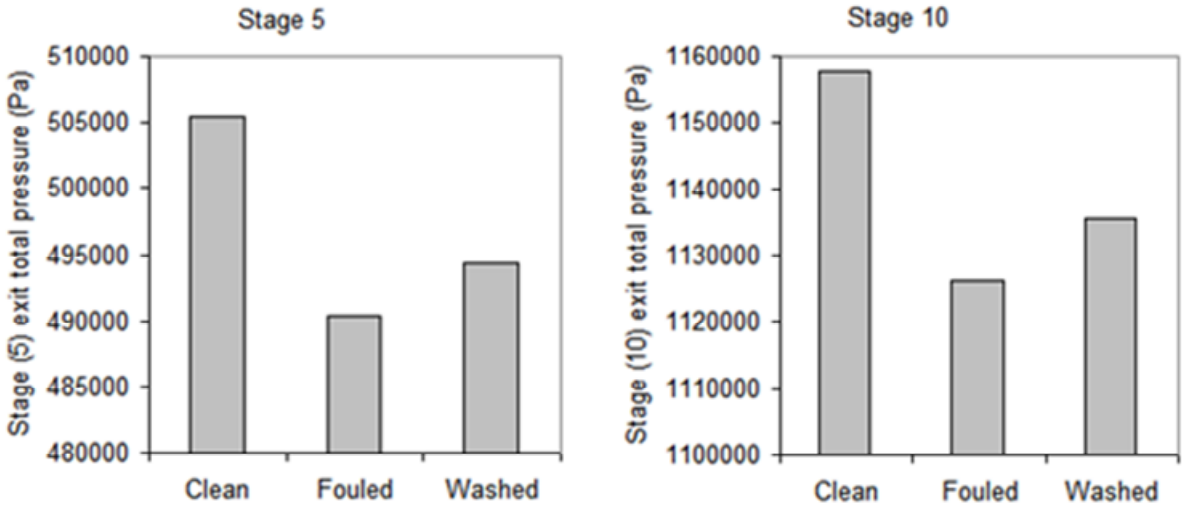
Stage 5
Stage (5) exit total pressure (Pa)
510000
505000
500000
495000
490000
485000
480000
Clean
Fouled
Washed
Stage 10
Stage (10) exit total pressure (Pa)
1160000
1150000
1140000
1130000
1120000
1110000
1100000
Clean
Fouled
Washed

Fig26.tiff

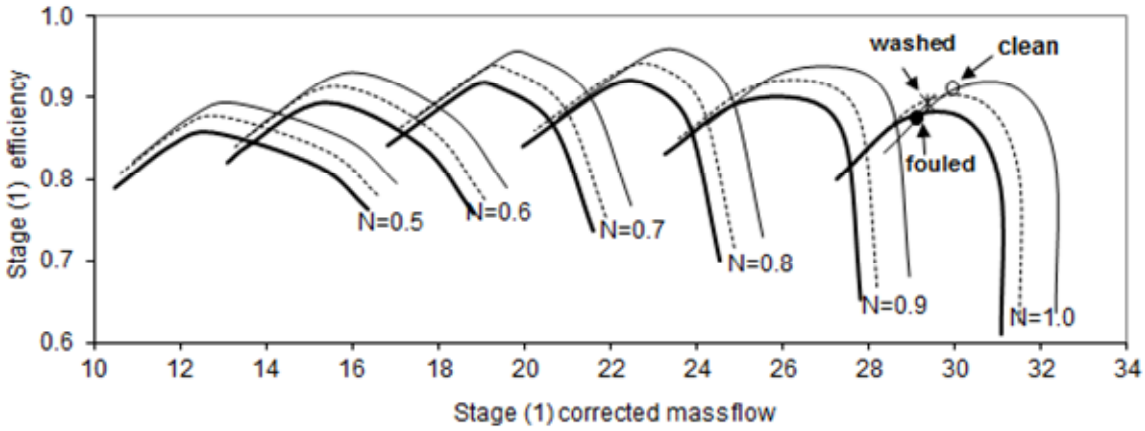
1.0
0.9
0.8
0.7
0.6
Stage (1) efficiency
10
12
14
16
18
20
22
24
26
28
30
32
34
Stage (1) corrected massflow
washed
clean
fouled
N=0.5
N=0.6
N=0.7
N=0.8
N=0.9
N=1.0

Fig27.tiff

APPENDIX

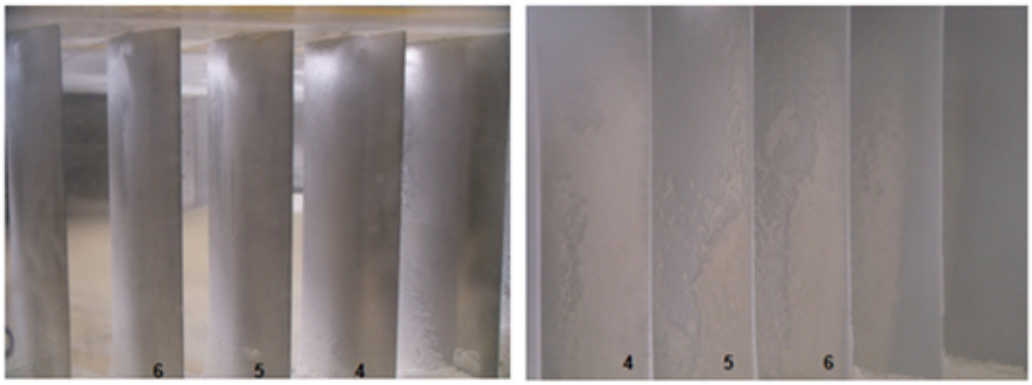

Fig28.tiff

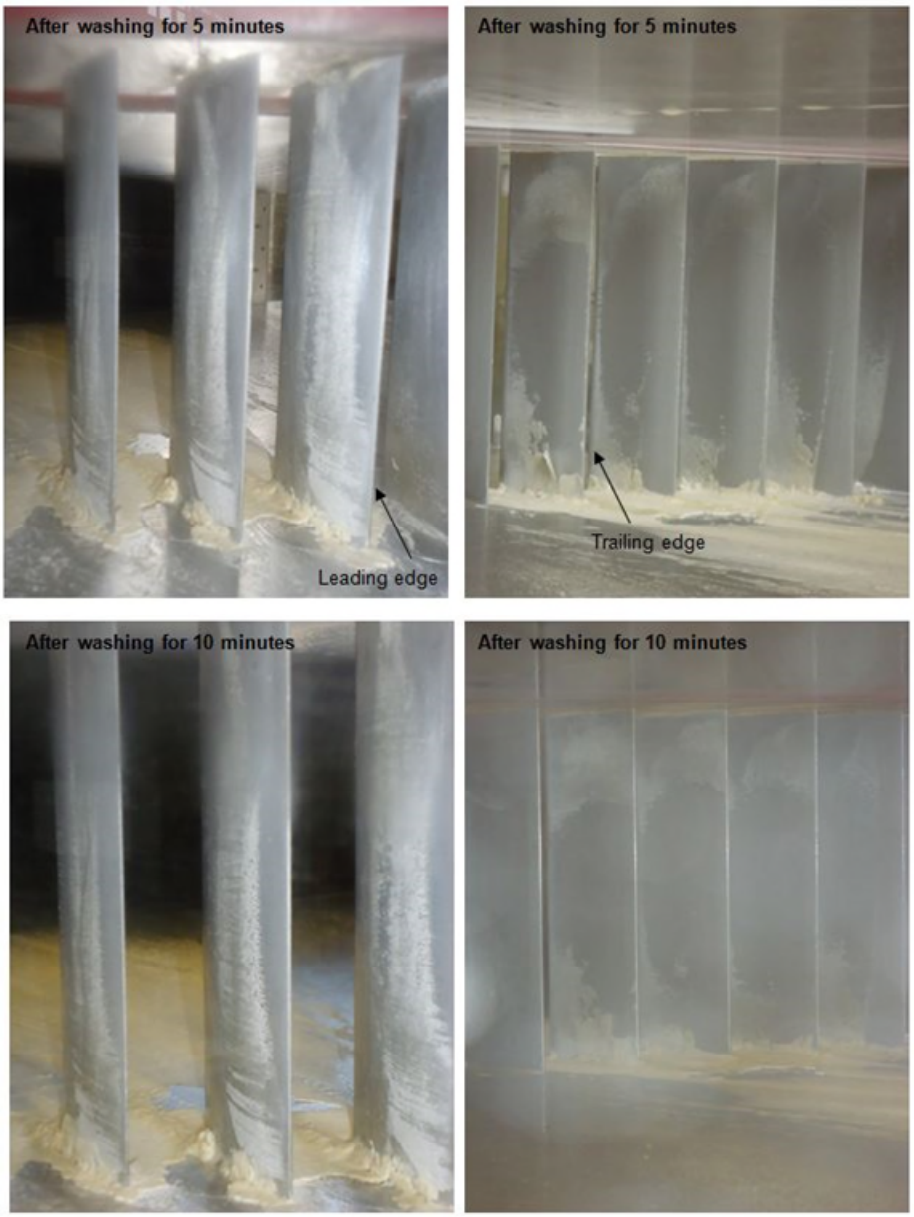

Fig29.tiff